HHS Public Access

Author manuscript

J Am Soc Echocardiogr. Author manuscript; available in PMC 2019 November 01.

Published in final edited form as:

J Am Soc Echocardiogr. 2018 November ; 31(11): 1168–1177.e1. doi:10.1016/j.echo.2018.06.009.

Three-Dimensional Mitral Valve Morphology in Children and Young Adults with Marfan Syndrome

Matthew A. Jolley, MD[1,3], **Peter E. Hammer, PhD**[2], **Sunil J. Ghelani, MD**[3,4], **Adi Adar, MD**[3], **Lynn A. Sleeper, ScD**[3,4], **Ronald V. Lacro, MD**[3,4], **Gerald R. Marx, MD**[3,4], **Meena Nathan, MD**[2,5], and **David M. Harrild, MD, PhD**[3,4]

[1]Department of Anesthesia and Critical Care Medicine and Division of Cardiology, Children's Hospital of Philadelphia, Philadelphia, PA, USA

[2]Department of Cardiac Surgery, Boston Children's Hospital, Boston, MA, USA

[3]Department of Cardiology, Boston Children's Hospital, Boston, MA, USA

[4]Department of Pediatrics, Harvard Medical School, Boston, MA, USA

[5]Department of Surgery, Harvard Medical School, Boston, MA, USA

Abstract

Background-—Mitral valve prolapse (MVP) is common in children with Marfan syndrome (MFS) and is associated with varying degrees of mitral regurgitation. However, the 3-dimensional (3D) morphology of the mitral valve (MV) in children with MFS and its relation to degree of mitral regurgitation (MR) are not known. The goals of this study were to describe the 3D morphology of the MV in children with MFS and to compare it to that of normal children.

Methods-—3D transthoracic echocardiography was performed in 27 patients (age 3–21 years) meeting revised Ghent criteria for MFS as well as 27 normal children matched by age (±1 year). The 3D geometry of the MV apparatus in mid-systole was measured, and its association with clinical and 2D echocardiographic parameters was examined.

Results-—Compared to age-matched controls, children with MFS had larger 3D annular area ($p<0.02$); smaller annular height-to-commissural-width ratio ($p<0.001$); greater billow volume ($P<0.001$); and smaller tenting height, area, and volume ($P< 0.001$ for all). In multivariate modeling larger leaflet billow volume in MFS was strongly associated with MR moderate or greater ($p< 0.01$). Intra- and inter-user variability of 3D metrics was acceptable.

Conclusions-—Children with MFS have flatter and more dilated MV annuli, greater billow volumes, and smaller tenting heights compared to normal controls. Larger billow volume is associated with MR. 3D MV quantification may contribute to identification of patients with MFS

Corresponding Author: Matthew A. Jolley MD, Children's Hospital of Philadelphia, 3401 Civic Center Blvd, Philadelphia, PA 19104, Phone 267-426-8794, JOLLEYM@email.chop.edu.

Disclosures: None

and other connective tissue disorders. Further study of 3D MV geometry and its relation to the clinical progression of MV disease is warranted in this vulnerable population.

Keywords

Marfan Syndrome; Mitral Regurgitation; Mitral Valve; Echocardiography (3-Dimensional)

Introduction

Cardiovascular manifestations in Marfan syndrome (MFS) include aortic root dilation and mitral valve prolapse (MVP). MVP is associated with varying degrees of mitral regurgitation (MR), which can be associated with progressive ventricular dilation and heart failure, and is the principal cause of morbidity and mortality in infants and small children with MFS.[1–4] Currently, two-dimensional (2D) qualitative assessments of the mitral valve (MV) are typically used to assess changes in valve function and structure over time.[5–7] Increasingly, however, the importance of characterizing the full three-dimensional (3D) nature of diseased valves is becoming recognized, both from a mechanical perspective and when considering surgical repair.[8–12] The non-planar ‘saddle shape’ of the MV, for example, has been shown to play a strong role in diminishing chordal stress and reducing the risk of chordal rupture.[11, 13, 14] This saddle shape cannot be reliably measured by 2D imaging; nor can many other annular and leaflet parameters.[15, 16]

As a consequence of suboptimal acoustic windows and reduced image quality, adult 3D mitral valve models are frequently constructed using transesophageal datasets acquired prior to or at the time of surgical repair. In children, however, acoustic windows are frequently superior to those of adults, and transthoracic imaging can be used successfully to construct valve models in a routine clinical outpatient setting.[17]

In patients with MFS, the 3D structure of the MV has not been characterized. Therefore, we sought to describe and quantify the 3D structure of the MV in a cohort of young patients with MFS using patient-specific models constructed from 3D transthoracic echocardiograms obtained during routine clinical outpatient visits. Moreover, we sought to compare the MV in MFS to valves from normal (non-MFS) age-matched controls. We hypothesized that the 3D structure of the MV might be associated with presence of significant MR.

Methods

Patients

An institutional database was reviewed to identify patients in a subspecialty Cardiovascular Genetics Clinic with the clinical diagnosis of MFS defined by revised Ghent criteria[18], in whom 3D imaging of the left ventricle and MV had been obtained as part of their clinical care.

Each MFS patient was matched to a normal control by date of birth ±1 year.[17] Briefly, 3D normal echocardiograms had been obtained as part of routine clinical care when structural or functional heart disease had been suspected, but was subsequently judged to be absent by the treating cardiologist. Specific criteria for inclusion in the normal cohort were: (1) referral for

clinical echocardiogram, (2) no history of congenital or acquired heart disease, (3) no more than trivial valvular regurgitation, (4) left ventricular end-diastolic volume normal or near normal (z-score between −2.5 and +2.5); (6) normal LV systolic function (ejection fraction > 55%); and (7) no other accompanying non-cardiac disease with potential cardiovascular impact.

The Committee on Clinical Investigation at Boston Children's Hospital approved this study.

Transthoracic Image Acquisition

3D images were acquired using Full Volume or 3D zoom mode, using 4-beat breath-held ECG-gated acquisitions when possible (breath holding was not typically feasible in infants and young children). Transthoracic X7 or X5 probes were used with the Philips IE33 and EPIQ ultrasound systems (Philips Medical, Andover, MA). Acquired datasets with significant stitch artifact or poor image quality were excluded from analysis. 2D volumes and ejection fraction, which were calculated using the 5/6 area length formula, were recorded from the clinical reports, as was the designation of the presence of MVP. 2D mitral annular anterior-posterior and lateral dimensions were recorded from the clinical reports if available; or were measured by one of us (DMH) if these data were missing. Mitral annular dimensions were expressed as z-scores as well as raw dimensions.

MV 3D Geometric Analysis

MV 3D models were constructed using the TomTec 4D MVA analysis package (v 2.3), running within the Image Arena 4.6 package (TomTec Imaging Systems, Unterschleisshem, Germany). Briefly, the MV analysis began with the identification of anatomic landmarks and selection of the early systolic frame (first frame with valve closed) and the end-systolic frames (last frame before the MV starts to open). A single mid-systolic frame midway between these two frames was chosen for static modeling and analysis of the valve. This phase was consistently well seen (and allowed direct comparison to previously published adult studies)[13, 19]. Annular and leaflet dimensions and shape were automatically generated by the software, using optical flow and pattern recognition with manual user correction when needed.[20, 21]

The following annular dimensions were recorded: annular circumference, anterior-posterior diameter, anterolateral-posteromedial diameter, commissural diameter, annular height, and annulus non-planar angle (Figure 1). Also recorded were 3D area and sphericity (defined as anterior-posterior diameter divided by the anterolateral-posteromedial diameter). Annular height to commissural width ratio (AHCWR), a measure of the saddle shape of the valve, was defined as the annular height divided by the annular commissural width and is expressed as a percentage.[11, 13]

Leaflet characteristics that were measured included: anterior leaflet area, posterior leaflet area, anterior leaflet length, posterior leaflet length, tenting height, tenting volume, and billow volume (Figures 2). Billow and tenting volumes were calculated in a custom fashion as these parameters are not calculated by the Tomtec analysis package (Figure 3). Specifically, bookmarks for each valve model were exported from the TomTec software in a DICOM format and were converted into a format suitable for import into MATLAB

(R2015b, The Mathworks Inc, Natick, MA, 2015). Using a custom-written program, a spline surface was constructed with minimal area that passed through all points on the annulus (i.e., the surface that a soap film would form across the annulus.) The volume between this reference surface and the leaflet surface generated by TomTec was then calculated using a discrete approximation to Gauss' divergence theorem. Volume on the atrial side of the reference surface was defined as billow volume; volume on the ventricular side of the reference surface was defined as tenting volume.

In order to allow comparisons between cases and controls across a wide range of patient ages and sizes in the study cohort, 3D measures were indexed by BSA (area and volume) and $BSA^{0.5}$ (lengths), as described in prior publications.[22]

Examples of mitral valve models of two MFS subjects and their age-matched controls are shown in Figure 4; these models highlight the flattened annular geometry and marked billow present in the mitral valves of the patients with MFS, compared to primarily tenting seen in the normal controls.

Statistics

Data are presented as median and interquartile range (IQR) unless otherwise stated. Statistical significance was defined as $p < 0.05$. Demographic characteristics of the MFS and control patients were compared using the Wilcoxon rank sum test. Despite frequency matching on age, we conservatively assumed that the groups were independent (not paired) since other important cohort differences may exist. The relationships of MV parameters to presence vs. absence of MVP and degree of regurgitation were assessed with the Wilcoxon rank sum and Kruskal-Wallis tests. Logistic regression was used to model presence vs. absence of MVP and ≥moderate MR as a function of other echocardiographic parameters, with step-wise selection to determine the independent correlates. Odds ratios and confidence intervals (CI) were calculated. Linear regression was used to explore relationships between continuous variables. Inter-observer and intra-observer reproducibility for 3D mitral measurements was assessed on a random subset of 16 subjects (8 MFS, and 8 controls). For intra-observer assessment the same observer (MAJ) re-measured all the parameters at least 1 month apart. For inter-observer assessment, a second observer (SJG) performed all measurements without knowledge of the results of the first observer. Intra-observer and inter-observer reproducibility was quantified using the intra-class correlation coefficient (ICC), which was generated using the two-way model for absolute agreement for average measures. In addition, mean absolute difference–defined as the average of the absolute value of the difference between the two values, divided by their mean (expressed as a percent)–was calculated for intra- and inter-observer measurements. Statistical analysis was performed using SAS 9.4 (SAS Institute Inc., Cary, NC, USA), and Stata version 13.1 (StataCorp, College Station, TX, USA).

Results

Patient Characteristics and 2D Echocardiogram Measurements

Demographic characteristics for the MFS and normal cohorts are shown in Table 1. The 2 groups differed statistically only in median systolic and mean blood pressures (MFS patients lower) and LVEDV z-score (MFS patients higher). Additional patient characteristics of the Marfan cohort and family history data are shown in Table 2. Both MVP and aortic root dilation were common in this cohort (70% and 89%, respectively). Among 2D echo measurements, MV lateral diameter (and z-score) was significantly larger among MFS patients than controls, as was MV A-P diameter (Table 3). Among Marfan patients the median aortic root z-score was 3.3 (IQR 2.6–4.5),

3D Annular and leaflet characteristics

Normalized 3D mitral annular characteristics are presented in Table 3 for MFS patients and controls. Compared to controls, children with MFS had significantly larger median AL-PM diameter, commissural diameter, annular circumference, and 3D annular area; AHCWR was smaller and annular non-planar angle was greater (indicating a flatter annulus), and MV annuli were less spherical.

Normalized 3D leaflet measurements are shown in Table 3. Compared to the normal cohort, children with MFS had larger median billow volume with smaller median tenting height, area, and volume. Leaflet lengths and areas did not differ between the two cohorts.

Larger LVEDV z-score was positively associated with normalized annular area and circumference ($R=0.73$, $p<0.0001$), and weakly associated with billow volume ($R= 0.31$, $p= 0.01$). Larger LVEDV z-score was also weakly negatively associated with AHCWR ($R= -0.31$, $p=0.02$) and normalized tenting height ($R= -0.29$, $p =0.04$). Aortic root z-score was positively associated with normalized annular area ($R = 0.50$, $p<0.0001$), valve circumference ($R=0.48$, $p <0.001$), the cube root of the billow volume ($R = 0.55$, $p<0.001$), and negatively associated with normalized tenting height ($R = -0.64$, $p< 0.0001$), tenting volume ($R= -0.39$, $p < 0.001$), and AHCWR ($R = -0.54$, $p < 0.0001$). Examining the relationship of 3D annular shape to leaflet structure, lower median AHCWR (a flatter annulus) was associated with smaller tenting volume ($R=0.47$, $p <0.001$) and weakly associated with greater billow volume ($R=0.33$, $p= 0.01$).

MV Prolapse and Mitral Regurgitation

Data from both cohorts were combined to form groups with ≥ moderate MR vs. <moderate MR; and MVP present vs. absent (Table 4). Compared to those with no MVP, subjects with MVP had larger median annular dimensions, areas, and non-planar angle, with lower AHCWR. Among leaflet parameters, MVP patients had smaller median tenting height, area, and volume, with larger median billow volume.

Compared to subjects with <moderate MR, those with ≥ moderate MR had larger median annular dimensions and area and non-planar angle, lower AHCWR, larger leaflet area parameters, increased billow volume, and decreased tenting volume. Normalized LVEDV z-

score was larger in the ≥ moderate MR group than the <moderate MR group (p<0.01). In the MFS only subgroup, there were similar associations of MR with MV annular and leaflet parameters although several metrics lost significance in this smaller cohort(Supplement Table 1).

Table 5 shows estimated odds ratios for MVP and MR grade moderate or greater by mitral valve parameters. Multivariate, stepwise selection showed billow volume to be the only independent predictor of moderate or greater mitral regurgitation (model p = 0.01, c-statistic 0.95). For MVP, only tenting height (OR 3.3, 95% CI 1.7–6.8, p<0.001), and annular area (OR 1.7, 95% CI 1.1–2.8, p=0.03) were independent predictors (model p<0.001, c-statistic 0.96).

Intra- and Inter-observer Variability

Intra- and intra-observer variability was generally acceptable (Table 6). Variables with the lowest inter-observer reproducibility (<0.75) included those which involved assessment of the non-planar shape of the valve such as non-planar angle, annular height, and tenting height, as well as posterior leaflet length. Further, billow and tenting volume had significant intra- and inter-observer variability.

Discussion

In this study we have quantitatively modeled the 3D morphology of the MV in children and young adults with MFS, compared these models to a group of normal patients, and showed large differences across an array of 3D valve and leaflet characteristics. Notably, valves in patients with MFS had substantially larger billow volumes, smaller tenting volumes, and larger annular dimensions. We have also showed associations between the 3D valve annulus and leaflet morphology and valve-specific patient morbidity, including MVP and MR.

Mitral Annular Shape

The shape of the normal and diseased MV in adults has been widely studied over the last two decades. Original work by Levine et al. characterized the saddle-shaped annulus of the MV.[11, 23] The normal range of AHCWR, with lower values representing a more planar shape, is 20–25% across a series of studies in adult humans.[24–27] Salgo et al. demonstrated in computational studies that there are mechanical benefits of the saddle-shaped mitral annulus to MV function.[11] Specifically, they demonstrated that leaflet stress is reduced when AHCWR is above 15% and minimal when AHCWR exceeds 20–25%. In vitro, the saddle-shaped annulus redistributes the forces on the chords by altering coaptation geometry, leading to an optimally balanced mechanical configuration.[14] In a recent study quantifying the annular shape in adult patients with MVP, Lee et al. showed that the clinical manifestation of leaflet stress in the form of chordal rupture was strongly associated with lower AHCWR.[13] Mean AHCWR was 23.7% in the normal group, 17.3% in the MVP+, MR- group, and only 13.2% in the MVP+, MR+ group. They also showed that in adult patients with MVP, a smaller AHCWR correlated inversely with leaflet billow volume, and AHCWR < 15% was independently associated with the presence of clinically significant MR. In our cohort, the median AHCWR was 20% in MFS patients, significantly lower than

in the normal cohort (24%) and at the bottom of the normal range reported in adults (20–25%).[28, 29] In our MFS patients with moderate or greater MR, the median AHCWR was 15%, exhibiting a similar trend to the adult study.

Leaflet Structure

While there are clear differences in the annulus in patients with MFS, the hallmark both visually and quantitatively in children with MFS was a larger MV leaflet billow volume compared to normal children. MVP is essentially the volume under the valve leaflet that is billowing past the annular plane into the left atrium in cross-sectional imaging. We have shown that billow in the mitral valves in normal patients is minimal. In contrast, the majority of patients with MFS had billow and many had significant amounts of billow exceeding the total tenting volume of the valve. Valve tenting orients the leaflets to better handle the systemic load imposed by ventricular contraction, and in prior work tenting metrics have been identified as important in prediction of adult MR.[30–33] Tenting height, area, and volume were all lower in our patients with MFS compared to normals.

Association of Structural Changes to MV Prolapse and Regurgitation

We sought to establish a relationship between 3D structural characteristics and valve function in this patient cohort. In univariate modeling of our population, a decrease in AHCWR by 5% (corresponding to annular flattening) was associated with a 4-fold increased odds of moderate or greater MR. Similarly, increased billow volume and decreased tenting volume were both highly associated with the risk of moderate or greater MR in univariate analysis. In multivariate modeling, billow volume was the only factor independently associated with moderate or greater MR. The effect size (odds ratio) was notably greater for billow and tenting volume than for simple annular dilation. Billow volume and tenting metrics were also highly associated with MVP; this would be expected, as these are essentially the quantitative 3D manifestation of the single plane visual assessment of MVP observed by conventional 2D echocardiographic techniques.

Mitral Valve Dysfunction in Marfan Syndrome – Potential Mechanisms

Marfan syndrome is caused by mutations in the *FBN1* gene which codes for the glycoprotein fibrillin-1.[34] While fibrillin-1 provides mechanical support to tissues, more recent studies have shown that fibrillin-1 plays a critical regulatory role in signaling of the cytokine, transforming growth factor beta (TGF-β). Absence of fibrillin-1 results in excessive amounts of activated TGF-β in the heart valves and aortic wall which is thought to lead to the clinical manifestations of the syndrome. Notably, in our MFS cohort, MV valve shape (billow volume and AHCWR) significantly correlated with aortic root z-score, supporting the idea that aortic enlargement and the MV abnormalities share a common pathogenesis.

The relationship between fibrillin and mitral valve abnormalities has been explored by Ng et al in a murine model of FBN1 deficiency.[35] In this work, the authors showed that mitral valve leaflets in the FBN1 deficient mice display myxomatous abnormalities associated with unchecked TGF-β activation leading to cell proliferation and reduced apoptosis. Notably, the mitral valve phenotype displayed by the FBN1-deficient mice was rescued by TGF-

β antagonists. We speculate that the resulting reduced structural integrity of the fibrous mitral annulus, leaflets, and supporting leaflet chordae could make the mitral valve complex in MFS more susceptible to leaflet billow and annular flattening. It is possible, for example, that in MFS, elongation and weakening of chordae would reduce the constraint on the commissural regions, allowing the annulus to assume a more planar shape.[14] A forward feedback mechanism may play a role as well; loss of annular saddle shape (lower AHCWR) may impose increased stress on chordae, further reducing their ability to support a normal annular shape.[11] These mechanisms may potentiate the deformation of intrinsically abnormal leaflets (manifesting as billow) due to excessive mechanical stress.[13] As the annulus flattens and dilates, the coaptation point moves toward the atrium, and the coaptation length decreases. Coverage of the valve area is maintained until the coaptation is depleted, resulting in a coaptation defect and mitral regurgitation. We have no means in our current study to validate these hypotheses related to the molecular and biophysical forces at play, and further investigation is needed. Further, it is unclear whether these changes are part of MVP of any etiology or age, or are at least partially unique to patients with MFS, and whether more subtle disruptions in TGF-β signaling contribute to the larger population of myxomatous mitral valve disease as a whole.[35]

Relevance and Potential for Clinical Utilization

Mitral valve dysfunction is present in 80% of patients with MFS and is the principal cause of morbidity and mortality in infants and young children with MFS.[1–4] Utilization of 3D echo-based modeling is well established in the adult literature for understanding leaflet abnormalities and planning surgical repair.[10, 36, 37] Given the high prevalence of leaflet and annular pathology in MFS children, application of modeling may be particularly useful in this young cohort due to superior transthoracic windows compared to older patients and may potentially influence repair strategy. For example, saddle-shaped annular rings have been utilized to restore the normal shape of the mitral valve in adults, and restoration of normal annular shape may be particularly relevant to the MFS population.[8, 11, 38, 39] Saddle-shaped rings have primarily been used in larger children due to their inability to account for somatic growth but absorbable annuloplasty rings have been described for younger patients.[40]

In the larger population of MFS patients not in need of imminent mitral valve repair, 3D modeling of the MV structure from clinical TTE may enable quantitative, longitudinal evaluation of the progression of mitral valve structural changes over time. Moreover, MFS is currently diagnosed by clinical manifestations as determined by the revised Ghent criteria. The 3D structural findings of the MV could be conceivably be relevant to the diagnosis of MFS, but will require validation in large cohorts of patients with MFS with and without MVP and patients with MVP without MFS.

Limitations

Our study is a small cohort of patients from one center, and the selection of MFS patients may be biased toward the more severe end of the spectrum due to their referral to a specialty tertiary center. The study was not blinded. There is a paucity of MFS patients without valvar regurgitation and/or prolapse, and no idiopathic MVP, non-Marfan MVP patients. While all

patients met revised Ghent criteria for MFS, *FBN1* gene testing was not performed in all subjects. Tomtec measures the "atrial surface" of the mitral valve and does not attempt to quantify the portion of the valve involved in coaptation, confounding assessment of true leaflet area and length. Small measurement differences based on manual placement of the coaptation point between the anterior and posterior leaflets or the annular reference points could result in differences in tenting heights. Similarly, annular height and bending angle suffered from lack of clear definition of the valve annulus visually. Important metrics, such as tenting volume, and billow volume suffered from relatively high inter-user variability. Improved automatic methods for annular and leaflet mapping will allow for standardization of the valve assessment, minimizing reliance on user input, and may reduce observer variability.[41, 42] Assessment of the valve structure was limited to a single mid-systolic frame, and further investigation of the dynamic changes in the annulus during all phases of systole and diastole is warranted. Not all 3D transthoracic images in MFS patients were amenable to modeling because of poor echocardiographic windows or patient motion in this pediatric cohort.

Conclusion

Children with MFS have flatter and more dilated MV annuli, increased billow volume, and decreased tenting volume compared to normal controls. Larger billow volume is strongly associated with degree of mitral regurgitation. Further study of 3D MV annular geometry and leaflet characteristics and their relationship to abnormalities in molecular signaling and the clinical progression of MV dysfunction is warranted in this vulnerable population.

Supplementary Material

Refer to Web version on PubMed Central for supplementary material.

Acknowledgments:

Thank you to Emily Harris for expert help in preparation of Figures and to Minmin Lu for statistical assistance.

Funding: This work was supported in part by the Higgins Family Noninvasive Imaging Research Fund at Boston Children's Hospital, grant R01 HL110997 from the National Institutes of Health and the Children's Hospital of Philadelphia Department of Anesthesia and Critical Care.

Abbreviations:

2D	2-Dimensional
3D	3-Dimensional
AHCWR	Annular height to commissural width ratio
BMI	Body Mass Index
BSA	Body Surface Area
CI	Confidence Intervals
Echo	Echocardiography

ICC	Intra-class correlation coefficient
IQR	Interquartile range
MFS	Marfan syndrome
MV	Mitral valve
MVP	Mitral valve prolapse
MR	Mitral regurgitation
TTE	Transthoracic echocardiography
LV	Left ventricular

References

[1]. Chan YC, Ting CW, Ho P, Poon JT, Cheung GC, Cheng SW. Ten-year epidemiological review of in-hospital patients with Marfan syndrome. Ann Vasc Surg 2008;22:608–12. [PubMed: 18562163]

[2]. Geva T, Hegesh J, Frand M. The clinical course and echocardiographic features of Marfan's syndrome in childhood. Am J Dis Child 1987;141:1179–82. [PubMed: 3673967]

[3]. Phornphutkul C, Rosenthal A, Nadas AS. Cardiac manifestations of Marfan syndrome in infancy and childhood. Circulation 1973;47:587–96. [PubMed: 4692214]

[4]. Morse RP, Rockenmacher S, Pyeritz RE, Sanders SP, Bieber FR, Lin A, et al. Diagnosis and management of infantile marfan syndrome. Pediatrics 1990;86:888–95. [PubMed: 2251026]

[5]. Lacro RV, Dietz HC, Sleeper LA, Yetman AT, Bradley TJ, Colan SD, et al. Atenolol versus losartan in children and young adults with Marfan's syndrome. N Engl J Med 2014;371:2061–71. [PubMed: 25405392]

[6]. Neptune ER, Frischmeyer PA, Arking DE, Myers L, Bunton TE, Gayraud B, et al. Dysregulation of TGF-beta activation contributes to pathogenesis in Marfan syndrome. Nat Genet 2003;33:407–11. [PubMed: 12598898]

[7]. Benke K, Agg B, Szilveszter B, Tarr F, Nagy ZB, Polos M, et al. The role of transforming growth factor-beta in Marfan syndrome. Cardiol J 2013;20:227–34. [PubMed: 23788295]

[8]. Levack MM, Jassar AS, Shang EK, Vergnat M, Woo YJ, Acker MA, et al. Three-dimensional echocardiographic analysis of mitral annular dynamics: implication for annuloplasty selection. Circulation 2012;126:S183–8. [PubMed: 22965981]

[9]. Mahmood F, Gorman JH, 3rd, Subramaniam B, Gorman RC, Panzica PJ, Hagberg RC, et al. Changes in mitral valve annular geometry after repair: saddle-shaped versus flat annuloplasty rings. Ann Thorac Surg 2010;90:1212–20. [PubMed: 20868816]

[10]. Mahmood F, Matyal R. A quantitative approach to the intraoperative echocardiographic assessment of the mitral valve for repair. Anesth Analg 2015;121:34–58. [PubMed: 26086507]

[11]. Salgo IS, Gorman JH, 3rd, Gorman RC, Jackson BM, Bowen FW, Plappert T, et al. Effect of annular shape on leaflet curvature in reducing mitral leaflet stress. Circulation 2002;106:711–7. [PubMed: 12163432]

[12]. Timek TA, Glasson JR, Lai DT, Liang D, Daughters GT, Ingels NB, Jr., et al. Annular height-to-commissural width ratio of annulolasty rings in vivo. Circulation 2005;112:I423–8. [PubMed: 16159857]

[13]. Lee AP, Hsiung MC, Salgo IS, Fang F, Xie JM, Zhang YC, et al. Quantitative analysis of mitral valve morphology in mitral valve prolapse with real-time 3-dimensional echocardiography: importance of annular saddle shape in the pathogenesis of mitral regurgitation. Circulation 2013;127:832–41. [PubMed: 23266859]

[14]. Jimenez JH, Soerensen DD, He Z, He S, Yoganathan AP. Effects of a saddle shaped annulus on mitral valve function and chordal force distribution: an in vitro study. Ann Biomed Eng 2003;31:1171–81. [PubMed: 14649491]

[15]. Izumo M, Shiota M, Kar S, Gurudevan SV, Tolstrup K, Siegel RJ, et al. Comparison of real-time three-dimensional transesophageal echocardiography to two-dimensional transesophageal echocardiography for quantification of mitral valve prolapse in patients with severe mitral regurgitation. Am J Cardiol 2013;111:588–94. [PubMed: 23206924]

[16]. Mahmood F, Hess PE, Matyal R, Mackensen GB, Wang A, Qazi A, et al. Echocardiographic anatomy of the mitral valve: a critical appraisal of 2-dimensional imaging protocols with a 3-dimensional perspective. J Cardiothorac Vasc Anesth 2012;26:777–84. [PubMed: 22841527]

[17]. Jolley MA, Ghelani SJ, Adar A, Harrild DM. Three-Dimensional Mitral Valve Morphology and Age-Related Trends in Children and Young Adults with Structurally Normal Hearts Using Transthoracic Echocardiography. J Am Soc Echocardiogr 2017;30:561–71. [PubMed: 28391001]

[18]. Loeys BL, Dietz HC, Braverman AC, Callewaert BL, De Backer J, Devereux RB, et al. The revised Ghent nosology for the Marfan syndrome. J Med Genet 2010;47:476–85. [PubMed: 20591885]

[19]. Pouch AM, Vergnat M, McGarvey JR, Ferrari G, Jackson BM, Sehgal CM, et al. Statistical assessment of normal mitral annular geometry using automated three-dimensional echocardiographic analysis. Ann Thorac Surg 2014;97:71–7. [PubMed: 24090576]

[20]. Veronesi F, Corsi C, Caiani EG, Sarti A, Lamberti C. Tracking of left ventricular long axis from real-time three-dimensional echocardiography using optical flow techniques. IEEE Trans Inf Technol Biomed 2006;10:174–81. [PubMed: 16445262]

[21]. Caban J, Joshi A, Rheingans P. Texture-based feature tracking for effective time-varying data visualization. IEEE Trans Vis Comput Graph 2007;13:1472–9. [PubMed: 17968099]

[22]. Sluysmans T, Colan SD. Theoretical and empirical derivation of cardiovascular allometric relationships in children. J Appl Physiol (1985) 2005;99:445–57. [PubMed: 15557009]

[23]. Levine RA, Handschumacher MD, Sanfilippo AJ, Hagege AA, Harrigan P, Marshall JE, et al. Three-dimensional echocardiographic reconstruction of the mitral valve, with implications for the diagnosis of mitral valve prolapse. Circulation 1989;80:589–98. [PubMed: 2766511]

[24]. Gorman JH, 3rd, Jackson BM, Enomoto Y, Gorman RC. The effect of regional ischemia on mitral valve annular saddle shape. Ann Thorac Surg 2004;77:544–8. [PubMed: 14759435]

[25]. Grewal J, Suri R, Mankad S, Tanaka A, Mahoney DW, Schaff HV, et al. Mitral annular dynamics in myxomatous valve disease: new insights with real-time 3-dimensional echocardiography. Circulation 2010;121:1423–31. [PubMed: 20231533]

[26]. Kaplan SR, Bashein G, Sheehan FH, Legget ME, Munt B, Li XN, et al. Three-dimensional echocardiographic assessment of annular shape changes in the normal and regurgitant mitral valve. Am Heart J 2000;139:378–87. [PubMed: 10689248]

[27]. Ryan LP, Jackson BM, Enomoto Y, Parish L, Plappert TJ, St John-Sutton MG, et al. Description of regional mitral annular nonplanarity in healthy human subjects: a novel methodology. J Thorac Cardiovasc Surg 2007;134:644–8. [PubMed: 17723812]

[28]. Bartels K, Thiele RH, Phillips-Bute B, Glower DD, Swaminathan M, Kisslo J, et al. Dynamic indices of mitral valve function using perioperative three-dimensional transesophageal echocardiography. J Cardiothorac Vasc Anesth 2014;28:18–24. [PubMed: 24011875]

[29]. Mihaila S, Muraru D, Piasentini E, Miglioranza MH, Peluso D, Cucchini U, et al. Quantitative analysis of mitral annular geometry and function in healthy volunteers using transthoracic three-dimensional echocardiography. J Am Soc Echocardiogr 2014;27:846–57. [PubMed: 24891260]

[30]. Song JM, Fukuda S, Kihara T, Shin MS, Garcia MJ, Thomas JD, et al. Value of mitral valve tenting volume determined by real-time three-dimensional echocardiography in patients with functional mitral regurgitation. Am J Cardiol 2006;98:1088–93. [PubMed: 17027577]

[31]. Tibayan FA, Wilson A, Lai DT, Timek TA, Dagum P, Rodriguez F, et al. Tenting volume: three-dimensional assessment of geometric perturbations in functional mitral regurgitation and implications for surgical repair. J Heart Valve Dis 2007;16:1–7. [PubMed: 17315376]

[32]. Toida R, Watanabe N, Obase K, Nagata Y, Yoshimura Y, Masuyarna H, et al. Prognostic Implication of Three-Dimensional Mitral Valve Tenting Geometry in Dilated Cardiomyopathy. J Heart Valve Dis 2015;24:577–85. [PubMed: 26897836]

[33]. Ryan LP, Jackson BM, Parish LM, Sakamoto H, Plappert TJ, St John-Sutton M, et al. Mitral valve tenting index for assessment of subvalvular remodeling. Ann Thorac Surg 2007;84:1243–9. [PubMed: 17888976]

[34]. Dietz HC, Cutting GR, Pyeritz RE, Maslen CL, Sakai LY, Corson GM, et al. Marfan syndrome caused by a recurrent de novo missense mutation in the fibrillin gene. Nature 1991;352:337–9. [PubMed: 1852208]

[35]. Ng CM, Cheng A, Myers LA, Martinez-Murillo F, Jie C, Bedja D, et al. TGF-beta-dependent pathogenesis of mitral valve prolapse in a mouse model of Marfan syndrome. J Clin Invest 2004;114:1586–92. [PubMed: 15546004]

[36]. Mahmood F, Karthik S, Subramaniam B, Panzica PJ, Mitchell J, Lerner AB, et al. Intraoperative application of geometric three-dimensional mitral valve assessment package: a feasibility study. J Cardiothorac Vasc Anesth 2008;22:292–8. [PubMed: 18375338]

[37]. Bouma W, Lai EK, Levack MM, Shang EK, Pouch AM, Eperjesi TJ, et al. Preoperative Three-Dimensional Valve Analysis Predicts Recurrent Ischemic Mitral Regurgitation After Mitral Annuloplasty. Ann Thorac Surg 2016;101:567–75; discussion 75. [PubMed: 26688087]

[38]. Jimenez JH, Liou SW, Padala M, He Z, Sacks M, Gorman RC, et al. A saddle-shaped annulus reduces systolic strain on the central region of the mitral valve anterior leaflet. J Thorac Cardiovasc Surg 2007;134:1562–8. [PubMed: 18023684]

[39]. Vergnat M, Levack MM, Jassar AS, Jackson BM, Acker MA, Woo YJ, et al. The influence of saddle-shaped annuloplasty on leaflet curvature in patients with ischaemic mitral regurgitation. Eur J Cardiothorac Surg 2012;42:493–9. [PubMed: 22351705]

[40]. Bautista-Hernandez V, Myers PO, Loyola H, Marx GR, Bacha EA, Baird CW, et al. Atrioventricular valve annular remodeling with a bioabsorbable ring in young children. J Am Coll Cardiol 2012;60:2256–8. [PubMed: 23103042]

[41]. Pouch AM, Aly AH, Lasso A, Nguyen AV, Scanlan AB, McGowan FX, et al. Image Segmentation and Modeling of the Pediatric Tricuspid Valve in Hypoplastic Left Heart Syndrome. Lect Notes Comput Sc 2017;10263:95–105.

[42]. Pouch AM, Wang H, Takabe M, Jackson BM, Gorman JH, 3rd, Gorman RC, et al. Fully automatic segmentation of the mitral leaflets in 3D transesophageal echocardiographic images using multi-atlas joint label fusion and deformable medial modeling. Med Image Anal 2014;18:118–29. [PubMed: 24184435]

Highlights

- The 3D structure of the mitral valve in children with Marfan syndrome(MFS) was compared to normal controls.
- Children with MFS have larger and flatter annuli, greater leaflet billow and less leaflet tenting.
- Greater leaflet billow volume was strongly associated with mitral regurgitation.

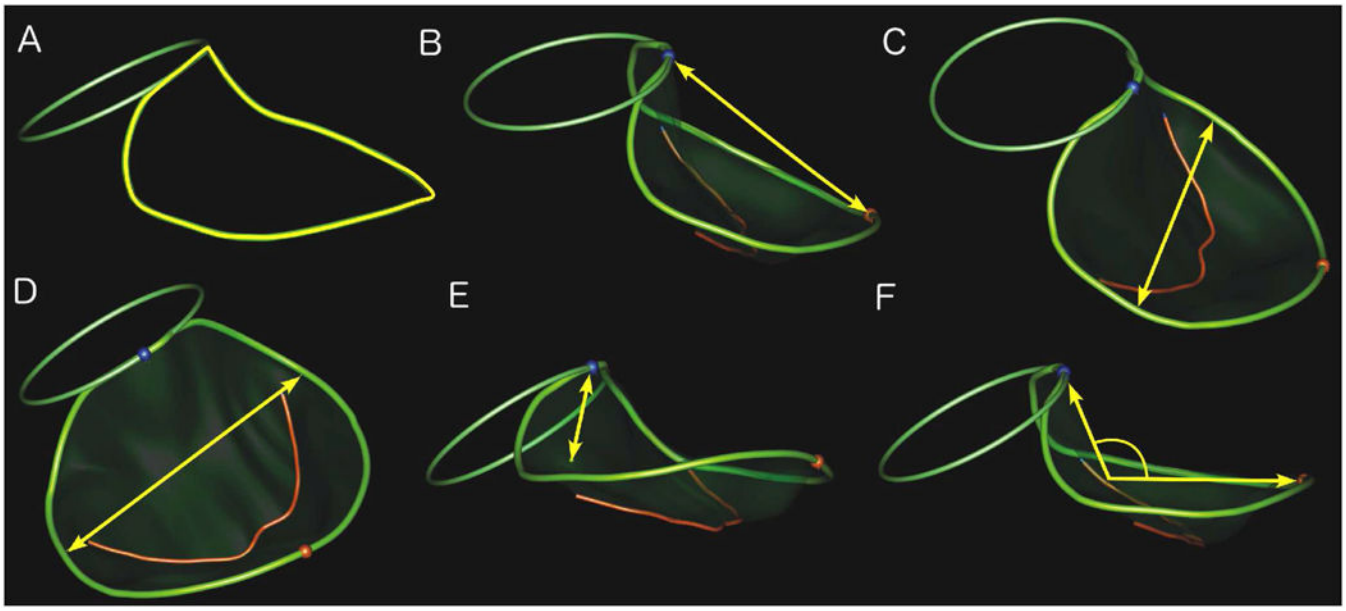

Figure 1: Mitral Annular Parameters

The mitral valve annulus (non-planar larger ring) and aortic valve annulus (smaller planar ring) are shown. Blue and red spheres indicate anterior and posterior points on the mitral annulus, respectively. The red curve conveys the coaptation line of the anterior and posterior leaflets. key measured variables are indicated in yellow.

A. Annular Circumference; B. Anterior-Posterior Diameter; C. Anterolateral-Posteromedial Diameter; D. Commissural Diameter; E. Annular Height; F. Annulus Non-planar angle.

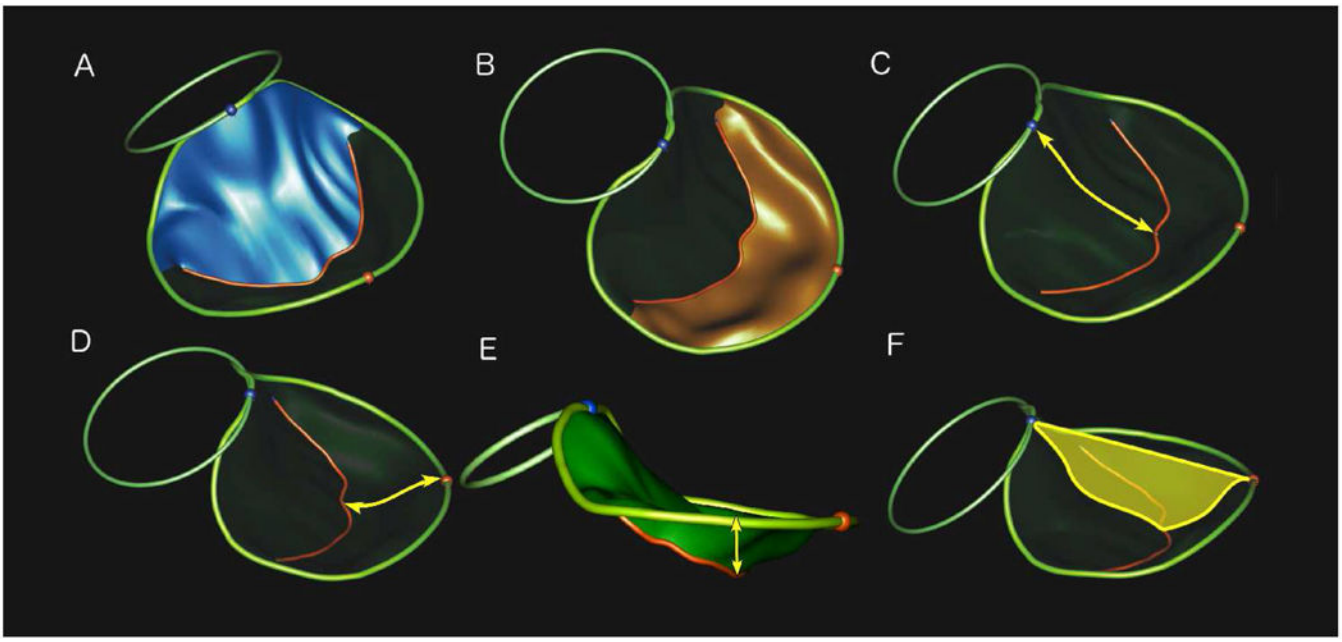

Figure 2. Leaflet Parameters.

The mitral valve annulus (non-planar larger ring) and aortic valve annulus (smaller planar ring) are shown. Blue and red spheres indicate anterior and posterior points on the mitral annulus, respectively. Red curve conveys the coaptation line of the anterior and posterior leaflets. Key measured variables are denoted in yellow, unless otherwise noted.

A. Anterior Leaflet Area (blue surface); B. Posterior Leaflet Area (orange surface); C. Anterior Leaflet Length; D. Posterior Leaflet Length; E. Tenting Height; F. Tenting Area (yellow surface).

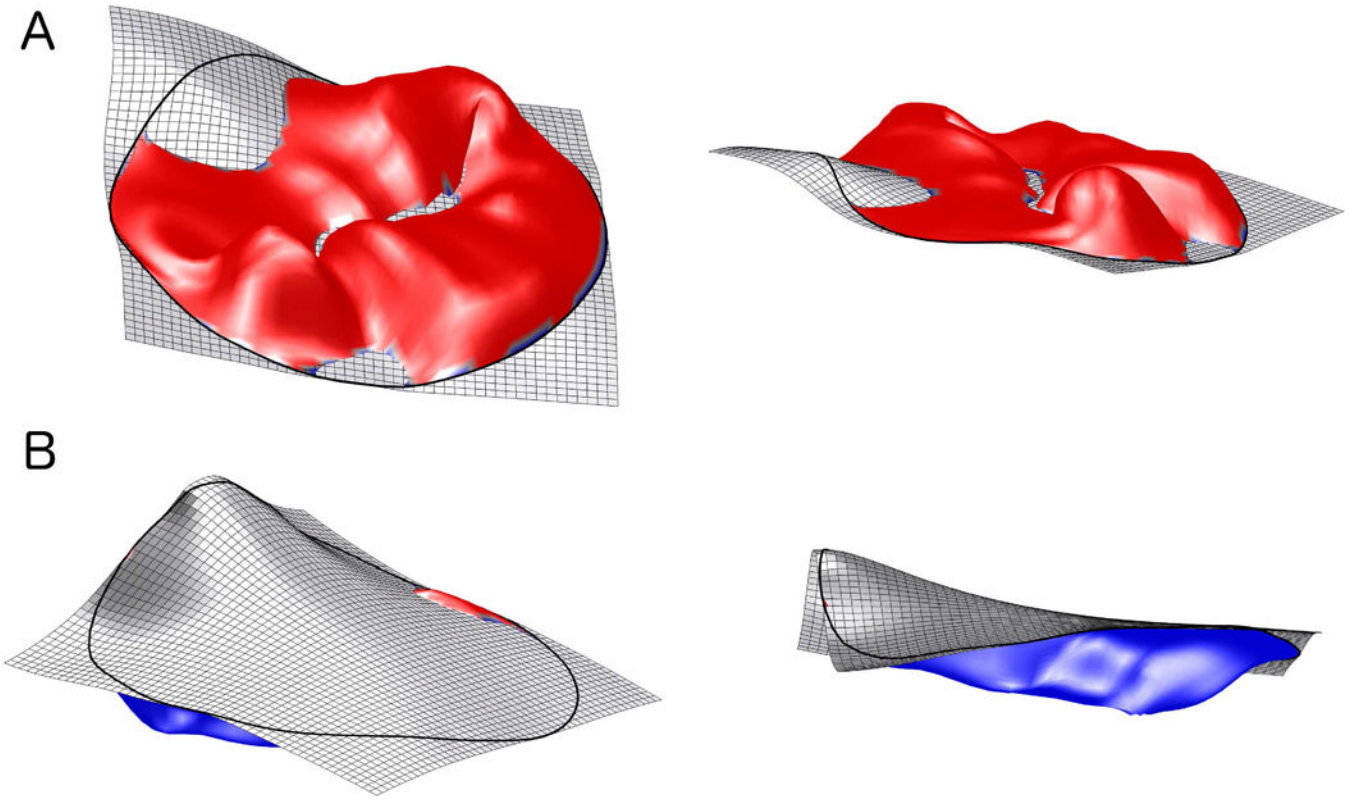

Figure 3: Billow and Tenting Volume.

A and B. Billow Volume (red surface; 2 perspectives). C and D. Tenting Volume (blue surface; 2 perspectives).

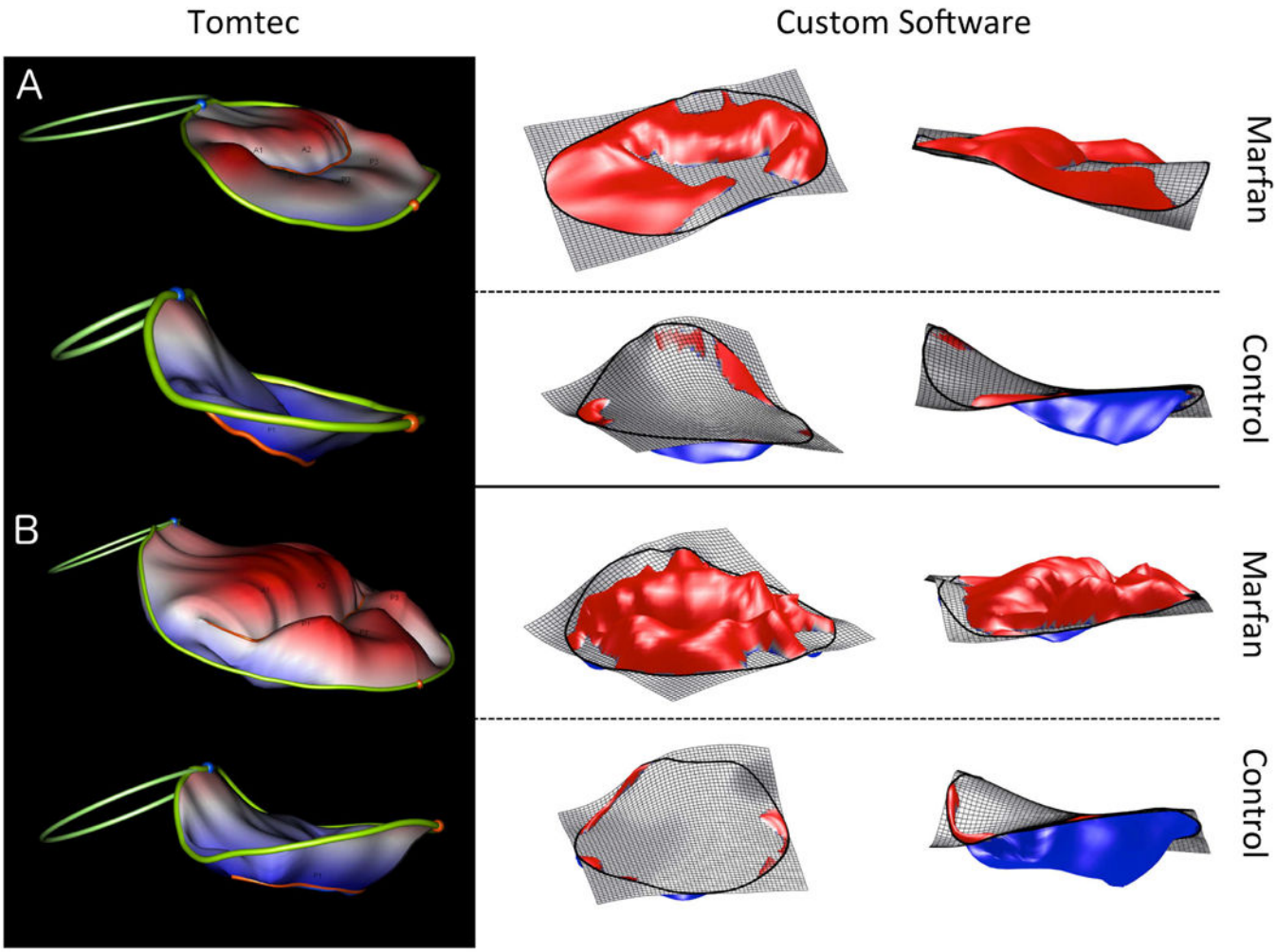

Figure 4: Example of comparison of Marfan patients (with severe billow) to typical controls.
A. 3-year-old Marfan patient vs control. B. 14-year-old Marfan patient vs control. In both examples billow is much more pronounced for the MFS patient.

Table 1:

Demographics

	Marfan		Control		p
n	27		27		
Female (%)	10	(37)	10	(37)	1
Age (y)	11.6	(9.3–16.6)	11.5	(8.2–16.8)	0.91
Weight (kg)	45.4	(34.3–66.3)	37.6	(26.2–63.0)	0.34
Height (cm)	164	(143–186)	145	(130–167)	0.07
BSA (m^2)	1.43	(1.16–1.80)	1.23	(0.95–1.70)	0.25
BMI (kg/m^2)	17.9	(16.2–19.2)	17.3	(16.0–21.4)	0.52
Heart Rate (bpm)	64	(57–72)	67	(59–77)	0.39
SBP (mmHg)	98	(90–103)	108	(102–115)	<0.001
DBP (mmHg)	55	(51–63)	59	(54–63)	0.22
MBP (mmHg)	65	(60–70)	72	(64–74)	0.05
Ejection fraction (%)	62	(58–66)	63	(58–66)	0.77
LVEDV (ml)	132	(102–177)	97	(63–152)	0.07
LVEDV z-score	1.8	(0.4–3.6)	0.6	(0.2–1.1)	0.01

Values are listed as median (IQR), P values calculated by two-sided Wilcoxon rank sum test Ejection fraction and ventricular volumes measured by 2D.

J Am Soc Echocardiogr. Author manuscript; available in PMC 2019 November 01.

Table 2:

Marfan Patient Characteristics (n=27)

Characteristic	n (%)	
Mitral valve prolapse	19	(70)
Mitral regurgitation (moderate or more)	5	(19)
Trivial/None	14	(51)
Mild	8	(30)
Moderate	4	(15)
Severe	1	(4)
Ectopia lentis	10	(37)
FBN1 mutation *	15	(56)
Aortic root z-score > 2	24	(89)
Family History		
Marfan syndrome	15	(56)
Aortic dissection	4	(15)
History of mitral disease	6	(22)
Family history of mitral surgery	5	(19)

* Of the 15 who had FBN1 testing, all had a pathogenic mutation.

Table 3:

Annulus and Leaflet Characteristics

	Marfan (n=27)		Control (n=27)		p
2D Annulus					
Lateral diameter (cm)	3.5	(3.0–3.8)	3.1	(2.6–3.5)	<0.001
Lateral diameter z-score	2.7	(1.2–4.2)	0.3	(−0.4–1.0)	<0.001
A-P diameter (cm)	2.9	(2.7–3.4)	2.7	(2.3–3.2)	0.05
A-P z-score	1.8	(0.6–2.8)	1.2	(0.7–1.7)	0.12
Area (2D; cm^2)	8.2	(6.3–9.5)	7.5	(4.6–8.5)	0.10
3D Annulus					
A-P diameter (cm/M)	2.8	(2.4–3.3)	2.6	(2.4–2.8)	0.12
AL-PM diameter (cm/M)	3.2	(2.8–3.6)	2.6	(2.4–2.8)	0.007
Width at commissure (cm/M)	3.2	(2.7–3.5)	2.9	(2.6–3.0)	0.007
Circumference (cm/M)	10.2	(8.9–11.3)	9.3	(8.3–9.8)	0.02
Area (3D; cm^2/M^2)	7.7	(5.8–9.1)	6.5	(5.1–7.2)	0.02
Annular height (cm/M)	0.6	(0.5–0.8)	0.7	(0.6–0.8)	0.046
AHCWR	20	(14–23)	24	(22–27)	<0.001
Non-planar angle (°)	149	(139–158)	138	(132–146)	0.006
Sphericity	0.89	(0.80–0.93)	0.93	(0.90–0.97)	0.049
3D Leaflets					
Total area (cm^2/M^2)	8.1	(6.4–9.9)	7.7	(6.4–8.1)	0.15
Anterior area (cm^2/M^2)	4.8	(4.0–5.3)	4.3	(3.7–4.8)	0.10
Posterior area (cm^2/M^2)	3.5	(2.4–5.1)	3.3	(2.6–3.6)	0.24
Anterior length (cm/M)	2.1	(1.8–2.2)	2.2	(2.0–2.3)	0.08
Posterior length (cm/M)	1.1	(0.9–1.4)	1.0	(0.9–1.1)	0.30
Tenting height (mm/M)	3.5	(2.0–4.9)	6.7	(6.1–7.3)	<0.001
Tenting area (cm^2/M^2)	0.6	(0.2–0.8)	1.1	(0.9–1.2)	<0.001
Billow volume (cc/M^2)	0.09	(0.03–0.37)	0.01	(0.00–0.02)	<0.001

	Marfan (n=27)		Control (n=27)		p
Tenting volume (cc)/M^2)	0.67	(0.21–0.96)	1.49	(0.87–1.72)	<0.001

Values are listed as median (IQR). P values calculated by Wilcoxon rank sum test, Two sided P > |Z|

A-P: Anterior-Posterior, AL-PM: Anterolateral-Posteromedial

AHCWR: Annular height to commissural width ratio, BSA: Body Surface Area

Table 4:

Mitral Regurgitation and MVP: Relationship to 3D Mitral Valve Parameters.

	MR ≥ Moderate n=5		MR ≤ Mild n=49		p	MVP n=19		No MVP n=35		p
Marfan Syndrome (n, %)	5	(100%)	22	(45%)	-	19	(100%)	8	(35%)	-
Annular Parameter										
AP-Diameter (cm/M)	4.1	(4.0–4.2)	2.7	(2.4–2.9)	0.007	3.1	(2.5–3.5)	5.8	(4.3–5.8)	0.003
AL-PM diameter (cm/M)	4.3	(4.1–4.5)	2.9	(2.6–3.2)	0.003	3.5	(2.8–4.3)	2.9	(2.6–3.1)	<0.001
Annular width at commissure (cm/M)	4.1	(4.0–4.2)	2.9	(2.6–3.2)	0.003	3.4	(2.7–4.1)	2.9	(2.6–3.0)	<0.001
Sphericity	0.86	(0.85–0.90)	0.92	(0.89–0.98)	0.14	0.90	(0.85–0.93)	0.92	(0.89–0.97)	0.22
Annulus circumference (cm/M^2)	12	(12.4–13.2)	9.6	(8.5–10.1)	0.006	10.7	(8.9–12.7)	9.3	(8.3–9.9)	0.002
Annulus area (cm^2/M^2)	11.9	(11.0–13.3)	6.8	(5.5–7.5)	0.008	8.6	(5.9–11.9)	6.5	(5.1–7.2)	<0.001
Annulus height (cm/M)	0.62	(0.46–0.68)	0.66	(0.53–0.77)	0.49	0.6	(0.5–0.7)	0.7	(0.6–0.8)	0.14
AHCWR	0.15	(0.14–0.15)	0.23	(0.20–0.26)	0.01	0.16	(0.14–0.22)	0.24	(0.21–0.27)	<0.001
Non-Planar Angle (°)	151	(149–167)	141	(134–150)	0.02	150	(144–162)	137	(132–146)	<0.001
Leaflet Parameter										
Total Leaflet Area (cm^2/ M^2)	13.1	(12.0–15.9)	**7.7**	(6.4–8.4)	0.009	9.1	(6.4–13.1)	7.7	(6.3–8.1)	0.006
Anterior Leaflet Area (cm^2/M^2)	6.9	(5.8–7.7)	4.3	(3.7–4.8)	0.004	4.8	(4.1–10.9)	6.5	(5.1–7.2)	0.021
Posterior Leaflet Area (cm^2/M^2)	7.3	(5.2–8.1)	3.3	(2.4–3.7)	0.008	4.1	(2.9–7.3)	3.2	(2.4–3.5)	0.018
Anterior Leaflet Length (cm/M)	2.2	(2.1–2.4)	2.1	(1.8–2.2)	0.09	2.1	(1.8–2.2)	2.2	(1.9–2.2)	0.94
Posterior Leaflet Length (cm/M)	1.6	(1.3–1.8)	1.0	(0.9–1.2)	0.02	1.2	(1.0–1.6)	1.0	(0.9–1.1)	0.026
Tenting Height (mm/M)	1.6	(1.6–3.2)	5.8	(4.1–6.8)	0.004	2.8	(1.6–4.9)	6.3	(5.4–7.0)	<0.001
Tenting Area (cm^2/M^2)	0.58	(0.12–0.74)	0.91	(0.58–1.12)	0.19	0.5	(0.1–0.8)	1.0	(0.7–1.2)	<0.001
Billow Volume (cc/M^2)	1.07	(0.61–3.3)	0.02	(0.01–0.05)	<0.001	0.13	(0.04–0.73)	0.01	(0.01–0.03)	<0.001
Tenting Volume (cc/M^2)	0.32	(0.12–0.94)	0.96	(0.67–1.57)	0.05	0.51	(0.13–0.96)	1.22	(0.82–1.61)	<0.001

Values are listed as median (IQR), P-values calculated by Wilcoxon rank sum test.

A-P: Anterior-Posterior, AL-PM: Anterolateral-Posteromedial

AHCWR: Annular height to commissural width ratio, BSA: Body Surface Area

Table 5:

Univariate Predictors of MVP and ≥ Moderate MR (n=54)

	Odds Ratio (95% CI)		p	c-statistic
MVP				
AHCWR (Per 5% decrease)	3.3	(1.6–6.6)	<0.001	0.79
Leaflet Billow Volume (Per 0.2cc/M^2 increase)	10.2	(1.4–72.8)	0.02	0.86
Leaflet Tenting Height (Per 1 mm/M decrease)	3.0	(1.7–5.1)	<0.001	0.91
Leaflet Tenting Volume (Per 0.5 cc/M^2 decrease)	2.8	(1.5–5.5)	0.002	0.79
3D Annular Area (Per 1cm2/ M^2 increase)	1.9	(1.2–2.8)	0.005	0.77
Moderate or Greater MR				
AHCWR (Per 5% decrease)	4.2	(1.3–13.8)	0.02	0.86
Leaflet Billow Volume (Per 0.2cc/M^2 increase)	2.8	(1.3–6.0)	0.01	0.95
Leaflet Tenting Height (Per 1 mm/M decrease)	2.1	(1.2–3.8)	0.01	0.89
Leaflet Tenting Volume (Per 0.5 cc/M^2 decrease)	3.0	(1.0–8.9)	0.05	0.77
3D Annular Area (Per 1cm^2/M^2 increase)	1.6	(1.2–2.3)	0.004	0.89

Modeled using univariate logistic regression

CI=Confidence Intervals

AHCWR=Annular Height to Commissure Width Ratio.

Table 6.

Inter- and Intra-observer variability for 3D Mitral Valve Measurements

Parameter	Intraobserver (n = 16)		Interobserver (n = 16)	
	Mean % Error ± SD	ICC	Mean % Error ± SD	ICC
AP-Diameter (cm)	6.30 ± 5.29	0.95 (0.87, 0.98)	5.65 ± 5.39	0.94 (0.85, 0.98)
AL-PM Diameter (cm)	3.30 ± 3.91	0.97 (0.92, 0.99)	4.69 ± 3.86	0.96 (0.90, 0.99)
Non-planar angle (deg)	2.16 ± 1.57	0.93 (0.82, 0.97)	5.63 ± 4.87	0.58 (0.16, 0.82)
Annulus circumference, 3D (cm)	3.85 ± 3.71	0.97 (0.92, 0.99)	4.52 ± 4.22	0.95 (0.87, 0.98)
Annular area, 3D (cm^2)	7.71 ± 7.63	0.97 (0.92, 0.99)	9.12 ± 8.52	0.95 (0.87, 0.98)
Annular height (cm)	10.17 ± 7.69	0.89 (0.73, 0.96)	9.21 ± 8.55	0.74 (0.42, 0.90)
Tenting volume (cc)	15.03 ± 14.36	0.95 (0.87, 0.98)	16.22 ± 15.46	0.94 (0.85, 0.98)
Tenting area (cm^2)	18.15 ± 17.63	0.95 (0.87, 0.98)	25.70 ± 35.14	0.80 (0.54, 0.92)
Tenting height (mm)	11.54 ± 8.96	0.93 (0.82, 0.97)	27.02 ± 38.09	0.56 (0.13, 0.81)
Commissural diameter	3.55 ± 4.26	0.97 (0.92, 0.99)	35.88 ± 31.99	0.96 (0.90, 0.99)
Anterior leaflet area	8.05 ± 8.38	0.96 (0.90, 0.99)	5.00 ± 4.18	0.94 (0.85, 0.98)
Posterior leaflet area (cm^2)	5.01 ± 4.09	0.99 (0.97, 1.00)	9.82 ± 9.26	0.83 (0.60, 0.93)
Anterior leaflet length (cm)	6.98 ± 5.99	0.88 (0.71, 0.95)	18.11 ± 11.50	0.80 (0.54, 0.92)
Posterior leaflet length (cm)	4.29 ± 4.63	0.96 (0.90, 0.99)	8.90 ± 7.56	0.58 (0.16, 0.82)
Billow volume (cc)	48.58 ± 36.92	0.96 (0.90, 0.99)	79.21 ± 52.02	0.95 (0.87, 0.98)

AP = anteroposterior; AL-PM = anterolateral-posteromedial.